DRAFT: MODELING AND MACHINE LEARNING AIDED ANALYSIS OF A MAGENTICALLY COUPLED BALL-DRIVE DESIGN

Biruk A. Gebre
Stevens Institute of Technology
Hoboken, NJ, USA

Kishore Pochiraju
Stevens Institute of Technology
Hoboken, NJ, USA

ABSTRACT

Ball driven mobility platforms have shown that spherical wheels can enable substantial freedom of mobility for ground vehicle. Accurate and robust actuation of spherical wheels for high acceleration maneuvers and graded terrains can however be challenging. In this paper a novel design for a magnetically coupled ball drive is presented. The proposed design utilizes an internal support structure and magnetic coupling to eliminate the need for an external claw-like support structure and enhance the performance of driven traction ball drives. A model of the proposed design is developed and used to evaluate the slip/no-slip operational window. Due to the high-dimensional nature of the parametrized model, the design space is sampled using randomly generated design instances and the data is used to train a support vector classification machine. Principal component analysis and feature importance detection are used to identify critical parameters that control the slip behavior and the feasible (no-slip) design space. The classification shows an increase in the feasible design space with the addition of, and increase in, the magnetic coupling force. Based on the results of the machine learning algorithm, FEA design tools and experimental testing is used to design a spherical magnetic coupler array configuration that can realize the desired magnetic coupling force for the ball drive.

INTRODUCTION

The continuous isotropic surface geometry of spherical wheels makes them an ideal choice for enabling unconstrained holonomic ground motion. While ball driven mobility platforms are a relatively new and emerging class for vehicle locomotion, renewed interest in research literature [1-7] has shown that they can exhibit agile omnidirectional maneuvering capabilities that are difficult or impossible to achieve using standard fixed or steered wheels. Spherical wheels also exhibit better ground traversal performance compared to other types of specialized wheels such as Omni-wheels and Mecanum wheels [8]. Implementation of spherical wheels for practical mobile ground robot applications can however be challenging due to difficulties with securely mounting and accurately actuating spherical wheels under various loading and terrain conditions. Since access to the entire surface of the spherical wheel is needed for omnidirectional ground traversal an axel cannot be used to actuate spherical wheels, unlike cylindrical shaped wheels. Methods of actuation that do not modify the surface geometry of the spherical wheels must therefore be used.

Existing implementation of ball driven mobility platforms found in literature include dynamically stable ballbots [1, 2] as well as statically stable multi-ball mobility platforms that utilize three or more spherical wheels [4, 3, 5]. An example of a traction ball drive used for a holonomic multi-ball mobility platform from the authors' prior work is shown in Figure 1. The ball drive shown in the figure utilizes an external "claw-like" support structure to incase and affix the spherical wheel to the chassis of the mobility platform. Freewheeling omnidirectional contacts located on the interior surface of the external support structure allow for free rotational motion and enable force transfer between the spherical wheel and the support structure. Actuation is achieved by applying traction forces to the exterior surface of the spherical wheels using actively driven Omni-wheels.

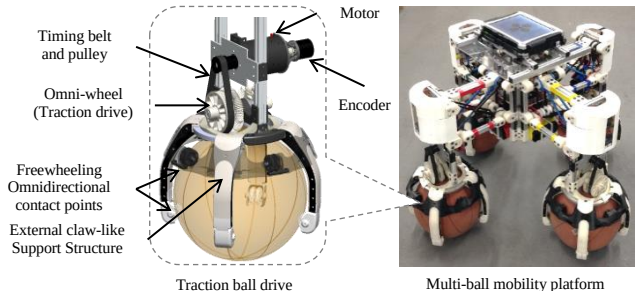

Figure 1. Example of traction ball drive used in authors' prior work [4] for a holonomic multi-ball mobility platform

The external support structure, which is utilized in many existing ball drive designs, has shortcoming related to reliability, efficiency, and the need for frequent maintenance when considered for long-term use. For example, dust particles and small debris picked up by the spherical wheel transfer to the contact points on the support structure during motion. When ball transfer units are used as the contact points for the support structure, this leads to excessive wear to the housing and ball bearings of the ball transfer units. This can deteriorate the performance of the ball transfer units by increasing the rolling resistance and causing the ball transfer units to periodically jam, similar to the ball transfer unit failures described in [9].

In [4] miniature Omni-wheels were used as an alternative to ball transfer units (as shown in Figure 1). The bearing surfaces of the miniature Omni-wheel are not exposed to the surface of the spherical wheel and were therefore less susceptible to the dust and debris picked up by the spherical wheels. The lower load carrying capacity of the miniature Omni-wheels did however result in the need for a larger number of contact points which increased the overall rolling resistance and adds to maintenance burden of the support structure.

Loss of traction between the drive wheel and the spherical wheel during high acceleration maneuvers is another issue encountered with existing traction ball drive designs. Slip occurs when the applied traction force exceeds the Coulomb static

friction force. This can result in motion errors for the platform, and cause abrasive damage to exterior surface of the spherical wheel. Even when using material combination with high friction coefficients loss of traction can still occur if there is insufficient normal force (e.g. when the weight distribution on the wheels shifts during motion) or if there is additional rolling resistance (e.g. when the spherical wheel if traversing over a large ground obstacle or going up a slope).

RELATED WORK

Interesting ball drive designs have been presented in recent literature. In [6 &10] Seyfarth et al. and Bhatia et al. presented a design for a spherical induction motor (SIM) drive mechanism for a ballbot named SIMbot. A hollow soft steel core spherical wheel with a Copper shell is used as a spherical rotor that is actuated, in all three rotational degrees of freedom, by six stators mounted on an external support structure. The design utilizes electromagnetic induction for actuation as opposed to physical traction forces used by existing ball drives. The SIM mechanism reduces the number of moving components, but does so at the cost of increased electrical complexity. The use of a solid metal spherical wheel may furthermore present a challenge for traversal of various ground terrains. An external support structure and ball transfer units are also still required to maintain a constant air gap between the spherical rotor and the stators.

In [7 & 11] Özgür et al. presented a design for a permanent magnet-assisted omnidirectional ball drive used for a small palm sized robot named Cellulo. Small spherical wheels with a ferromagnetic core are driven by permanent ring magnets for this design. The magnetostatic pull increases the static friction force between the drive rollers and the spherical wheels and allows for the transmission of larger traction forces for actuation. The design, as-is, however does not scale well for use in larger sized multi-ball mobility platforms due to the large weight and size of the ferromagnetic core spherical wheel and permanent magnet drive rollers that would be required.

In this paper a novel design for a magnetically coupled ball drive (MCBD) is presented. The design aims to improve on the reliability and the actuation efficiency of existing spherical wheel ball drives. The basic concept of the magnetically coupled ball drive is first presented, followed by a dynamic model of the system. The multi-dimensional design space of the parametrized model is then analyzed using machine learning techniques to determine effects of the magnetic coupler on the feasible no-slip design space. Finite element analysis is then used to design a magnetic coupler based on the results of the machine learning algorithm. The performance of the magnetic coupler is experimentally verified and preliminary work on the development of a proof-of-concept prototype for the MCBD concept is also presented.

MAGNETICALLY COUPLED BALL DRIVE

Concept

The MCBD concept proposed in this paper utilizes an internal support structure that rolls along the interior surface of the spherical wheel and is held in place using magnetic force. A 2D schematic of the concept is shown in Figure 2. The magnetic force is applied directly above the spherical wheel and Omni-wheels on either side of the magnet are used to actuate the spherical wheel. Lubricated ball transfers located on the exterior of the support structure allow the spherical wheel to freely rotate about the internal support structure. The ball transfers also maintain a small air gap between the permanent magnet located at the top of the internal support structure and the interior surface of the spherical wheel.

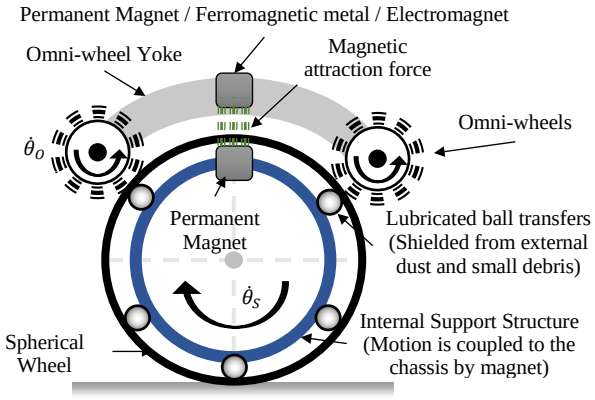

Figure 2: 2D schematic of magnetically coupled ball drive (MCBD) concept

The rotational motion of the internal support structure is locked to the motion of the platform using magnetic force applied from the center of the Omni-wheel yoke. The motion of the internal support structure will therefore be coupled to the motion of the platform chassis. Translational forces are transferred between the platform and the spherical wheel through the contact forces between Omni-wheels and the spherical wheels as well as through the non-contact magnetic force applied to the internal support structure.

A number of design objectives are achieved by utilizing an internal support structure. First the contact points between the internal support structure and the spherical wheel will remain shielded from external dust and small debris picked up on the exterior surface of the spherical wheel. This enables the use of ball transfers as the contacts for the internal support structure and also allows for the use of lubrication to minimize friction and rolling resistance. Secondly the magnetic force increases the normal force applied to the drive wheels which allow for the transmission of higher traction forces. Control of the magnetic coupling force should also enable dynamic adjustment of the no-slip region during motion.

By placing the support structure internally more of the exterior surface of the spherical wheel is also exposed which allows for easier traversal of ground obstacles and terrain. The internal support structure also increases the mass of the spherical wheel which improves the stability of the platform by lowering its center of gravity. The rotational inertia of the spherical wheel is however not affects as the rotation of the internal support structure is magnetically locked.

Dynamic Model

The free body diagram used for the 2D model of the MCBD concept is shown in Figure 3 (equations are omitted due to space constraints). For this model, slip occurs if the traction forces for either the left or the right Omni-wheels exceed the Coulomb static

friction force (i.e. $F_{Tl} > \mu_{OS}N_{Ol}$ or $F_{Tr} > \mu_{OS}N_{Or}$) where μ_{OS} is the static friction coefficient between the spherical wheel and the Omni-wheels. A total of 12 force and torque balance equation can be generated from the free body diagrams in Figure 3 (three for the spherical wheel, three for each of the two Omni-wheels and three for the yoke). Matlab's symbolic toolbox is used to simultaneously solve the equations using the parameters listed in Table 1 as symbolic variables. The slip function for the left and right Omni-wheel are calculated as $|F_{Tl}|/\mu_{OS}N_{Ol}$ and $|F_{Tr}|/\mu_{OS}N_{Or}$ respectively. Slip occurs if either slip function ≥ 1.

Table 1: symbolic variables solved for in Matlab

$\boldsymbol{F_F}$	Friction force from ground contact
$\boldsymbol{F_{Rxl}}$	x reaction force for left Omni-wheel axle
$\boldsymbol{F_{Rxr}}$	x reaction force for right Omni-wheel axle
$\boldsymbol{F_{Ryl}}$	y reaction force for left Omni-wheel axle
$\boldsymbol{F_{Rxy}}$	y reaction force for right Omni-wheel axle
$\boldsymbol{F_{Tl}}$	Traction force from left Omni-wheel
$\boldsymbol{F_{Tr}}$	Traction force from right Omni-wheel
$\boldsymbol{N_G}$	Normal ground reaction force
$\boldsymbol{N_{Ol}}$	Normal reaction force for left Omni-wheel
$\boldsymbol{N_{Or}}$	Normal reaction force for right Omni-wheel
$\boldsymbol{\tau_{RY}}$	Reaction Torque for Yoke
$\boldsymbol{\ddot{\theta}_S}$	Angular acceleration of spherical wheels

The resulting lengthy slip functions are a six-dimensional parametric space composed of; the inclination angle (β), the left and right Omni-wheel torques (τ_{Ol} and τ_{Or}), the magnetic coupling force (F_M), the load applied onto the ball drive by the platform (w_p), and the static friction coefficient between the Omni-wheels and the spherical wheels (μ_{OS}). Due to the length and high dimensionality of these slip functions machine learning technique were employed to analyze the feasible design space.

Exploration of design space using ML

A minimum and maximum value is defined for each parameter of the slip functions to define the range for the design space we would like to explore (Table 2). The dynamic model is then used to randomly sample the design space with 50,000 design instances for 7 specific values of F_M (0N, 50N, 100N, 150N, 200N, 250N, and 500N). Using the constants in Table 3 the slip functions are calculated for each of these design instances and labeled as 1 or 0 to indicate slip or no-slip respectively.

Table 2: Design space for MCBD

Parameter	Variable	Min value	Max value	Units
X1	$\boldsymbol{\beta}$	$-\pi/8$	$\pi/8$	Radians
X2	$\boldsymbol{\tau_{Ol}}$	0	10	Nm
X3	$\boldsymbol{\tau_{Or}}$	0	10	Nm
X4	$\boldsymbol{F_M}$	0	500	N
X5	$\boldsymbol{W_p}$	0	200	N
X6	$\boldsymbol{\mu_{OS}}$	0.2	1.2	-

Table 3: Constants used for exploration of design space

$r_O\ (m)$	$r_S\ (m)$	$m_O\ (Kg)$	$m_s\ (Kg)$	$m_Y\ (Kg)$	$\varphi_O\ (rad)$
0.0508	0.1016	0.5	2.5	2	$\pi/4$

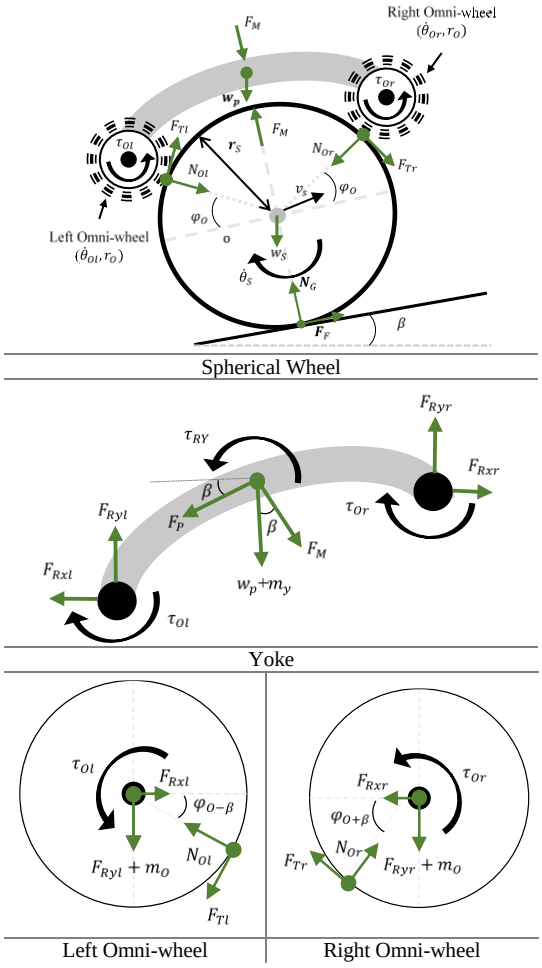

Figure 3: Free body diagram for simplified 2D model of magnetically coupled ball drive

A support vector classifier machine [13] was trained on the dataset using a Radial Basis Function (RBF) kernel. The feature importance scores of the parameters for seven F_M values that were evaluated is shown in Figure 4. The classifier was able to achieve a prediction accuracy of 92.4% with C=1000 and Gamma = 0.001 (recall accuracy 0.912 +/- 0.009). Figure 5 examines the support vector classifier trained on a 10000 sample training set obtained by randomly sampling the six features and labeling each sample with a binary slip/no slip label. The figure shows the classifier performance on two 2D planes, (X_2,X_5) and (X_1,X_6). The classifier effectively divided the design space into slip (infeasible/red) and no-slip (feasible/blue) regions. The figures also shows that the magnetic coupling force substantially increases the feasible set of designs.

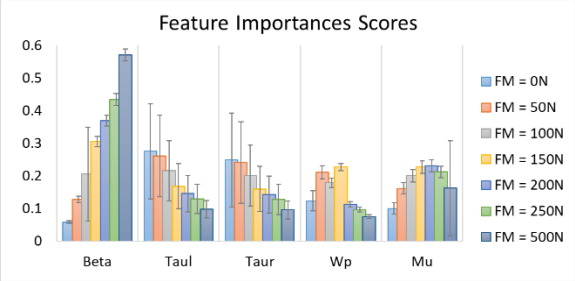

Figure 4: Feature importance scores of design space parameters for the seven F_M values evaluated

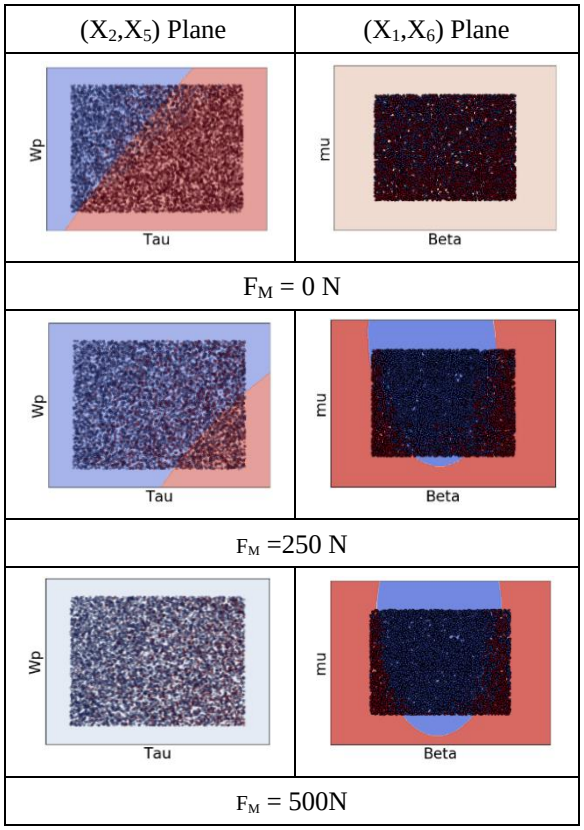

Figure 5: Slip (red) and No-Slip (Blue) surfaces based on two feature classification with 10,000 training samples.

Next, Principal Component Analysis (PCA) was performed on a scaled feature space. Figure 6 shows support vector classification and the delineation of feasible (blue) and infeasible (red) spaces with respect to three principal components for F_M = 250N and 500N which resulted in an increase of the feasible space from 53.1% to 88%

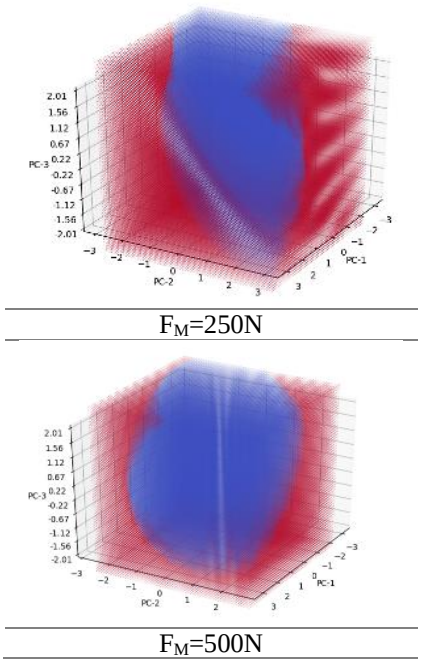

Figure 6: Feasible design space (blue) shown with respect to three principal components. The increase in F_M from 250N to 500N is shown to increse the feasible space by 35%.

MAGNETIC COUPLER DESIGN

The magnetic coupler works in conjuction with the Omni-wheels to function as a virtual axle for the spherical wheel. As shown from the results of the machine learning algorithm, strong magnetic coupling allows for a larger feasible operational range. A large F_M value can however also increase the rolling resistance of the Omni-wheel rollers and reduce the actuation efficiency of the ball drive. A controllable magnetic force is therefore desirable so that the strength of the magnetic coupler can be dynamically adjusted as needed during motion.

A pair of single magnets, as shown in MCBD concept schematic in Figure 2, was first evaluated as this presented the simplest implementation of the magnetic coupler. EMS software from EMworks [12] was used to run a magnetostatic FEM simulation for a pair of 25.4mm x 25.4mm cylindrical N52 NdFeB magnets. Accounting for the 7.62mm thickness of the spherical wheel and the minimum air gap of 2.54mm between the magnets and the spherical wheel surfaces resulted in a minimum coupling distance of 12.7mm between the pair of magnets. The magnetic flux density and F_M values at three coupling distances for the single pair of magnets is shown in Figure 7.

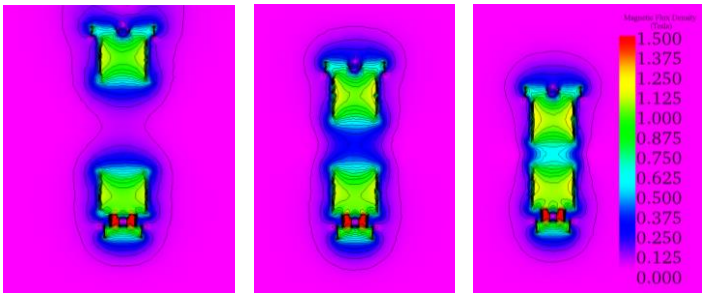

Distance = 50.8mm
FM = 2.06N

Distance = 25.4mm
FM = 19N

Distance = 12.7mm
FM = 67N

Figure 7: Magnetic flux density and corresponding F_M values for a pair of 25.4mm x 25.4mm cylindrical N52 NdFeB magnents at three coupling distanes.

As shown in the figure the magnetic coupling force increases exponentially as the coupling distance decreases. While the 25.4mm cylindrical N52 NdFeB magnets used for the simulation are very powerful and capable of exerting >500 N of pull force when in contact, at the minimum coupling distance of 12.7mm they are not able to generate the minimum desired coupling force of 100N. Larger sized magnets, while capable of generating the desired forces would also have larger magnetic fields that would extend further and exert influence beyond the diameter of the spherical wheel.

The use of magnetic arrays was therefore evaluated as an alternative to larger magnets. Two magnetic coupler array (MCA) designs that utilized 5 pairs of the 25.4mm N52 NdFeB cylindrical magnets were tested. The first was a collinear MCA where 4 additional pair of magnets were uniformly patterned around the vertical axis at an angle of 22.5º (Figure 8 (a)). The second was an opposing MCA design which had a similar layout to the collinear MCA design with the exception that the central pair of magnet had an opposite magnetic polarity to the 4 surrounding pair of magnets (Figure 8(b)). The magnetic flux density results from the magnetostatic FEM simulations of the two MCA designs performed using EMS software at the minimum distance of 12.7mm are shown in Figure 9.

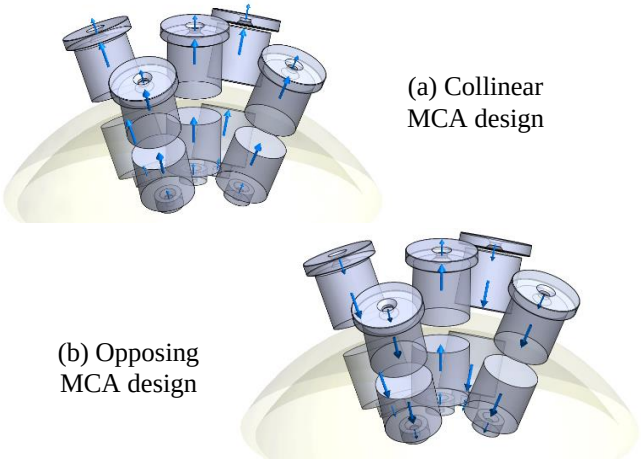

(a) Collinear MCA design

(b) Opposing MCA design

Figure 8: Magnetic Coupler array (MCA) designs evaluated for MCBD concept

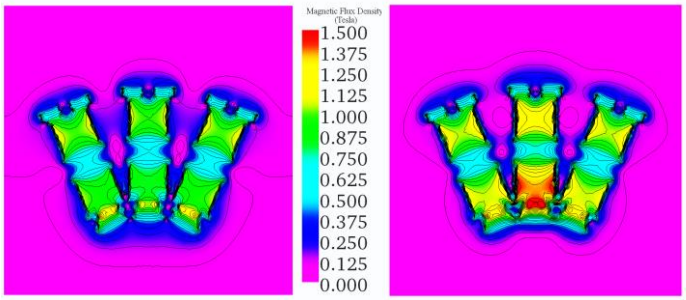

Figure 9: Magnetic flux density for the collinear and opposing MCA designs. Significant increase in magnetic flux desnity is acheieved using the opposing MCA design. Extent of magnetic field is also more contained using opposing MCA design.

Both arrays were able to generate forces in the desired 100N – 500N range. The opposing MCA design was able to generate a larger magnetic attraction force at the minimum coupling distance of 12.7mm as the magnetic field lines were concentrated at the central pair of magnets resulting in a much larger magnetic flux density. The Collinear MCA had a more uniform lower magnetic flux density with magnetic field lines that extended further out than the Opposing MCA design. The results from the simulations were verified experimentally using a Mark-10 motorized force test stand. Both MCA designs as well as the single cylindrical N52 NdFeB magnet pair shown in Figure 7 were tested. The results are shown in Figure 10.

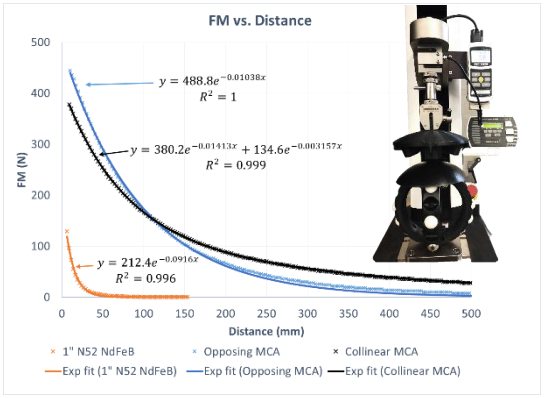

Figure 10: Experimental verification of simulation results using motorized force test stand

The test results concur with the simulation results and clearly shows that the single magnet pair would not be able to generate sufficient coupling force on its own. As expected the opposing MCA design was able to generate larger forces at shorter coupling distance and decayed at a faster rate than the Collinear MCA. The Opposing MCA was able to generate an F_M of 436N at the minimum coupling distance of 12.7mm and force of 100N at a distance of 153mm. An exponential fit of the data was used to generate the following equation which calculates the coupling distance (d) required to produce the desired coupling force F_M for the opposing MCA design.

$$d = ln(F_M/488.8)/-0.01038 \qquad (1)$$

PROOF-OF-CONCEPT PROTOTYPE

A small scale prototype of the MCBD concept using a 63.5mm radius spherical wheel and 25.4mm Omni-wheels has been built and manually tested to verify the feasibility of the claw-less MCBD design. A larger prototype using the spherical wheel and Omni-wheel dimensions used in the model is currently being built and will be instrumented in the future to further test and verify the model. A challenge in realization of the MCBD concept has been in the fabrication of a spherical wheel that can allow for the placement of an internal support structure. For the proof-of-concept prototype Photopolymer jetting Additive Manufacturing technology is being utilized to fabricate the components for the spherical wheel assembly as shown in Figure 11.

Photopolymer jetting is a multi-material 3D printing process therefore a range of digital material will be used to construct the spherical wheel ranging from soft rubber-like material for the outer layer of the spherical wheel with a high static friction coefficient to a harder polypropylene-like material on the inner layer to provide for a lower rolling resistance for the bearing balls of the internal support structure and higher load bearing capacity.

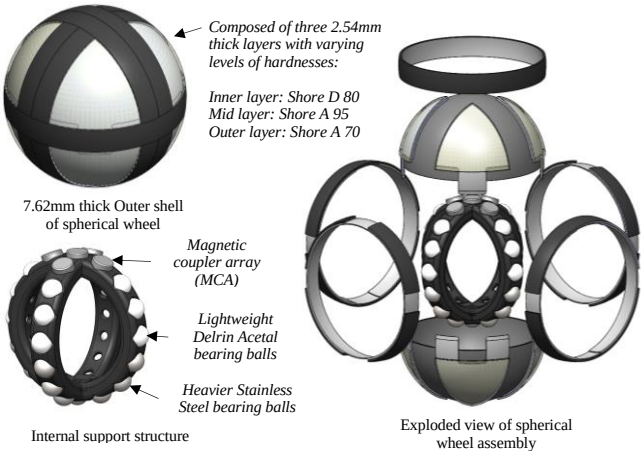

Figure 11: Design of spherical wheel for MCBD proof-of-concept prototype

CONCLUSION

In this paper a novel magnetically coupled ball drive is presented. A model of the proposed design is evaluated using machine learning techniques to explore the high dimensional design space. Classification results from the machine learning algorithm were able to show that the feasible no-slip design space for a traction ball drive can be substantially increased through the addition of strong magnetic coupling force. Results from the machine learning algorithm coupled with finite element analysis and experimental verification were used also used to generate a design for a magnetic coupler array capable of generating a controllable magnetic coupling force within the desired range.

The MCBD ball drive presented in this paper can be utilized in number ball drive configuration a shown in [15]. Further development and testing is still needed to experimentally verify the performance gains that can be attained using the MCBD concept and is planned for future work. While many practical challenges still remain in the implementation of spherical wheels for mobile ground vehicles the MCBD concept presented in this paper aims to address some of these challenges in a step towards realizing the full potential of spherical wheels for enabling agile holonomic motion for ground vehicles.

REFERENCES

[1] U. Nagarajan, G. Kantor and R. Hollis, "The Ballbot: An Omnidirectional Balancing Mobile Robot," *The International Journal of Robotics Research*, vol. 33, no. 6, pp. 917-930, 2014.

[2] L. Hertig, D. Schindler, M. Bloesch, C. D. Remy and R. Siegwart, "Unified State Estimation for a Ballbot," in *Robotics and Automation (ICRA), 2013 IEEE International Conference on.*, Karlsruhe, Germany, 2013.

[3] L. Ferrière, G. Campion and B. Raucent, "ROLLMOBS, a new drive system for omnimobile robots," *Robotica* , vol. 19, no. 1, pp. 1-9, 2001.

[4] B. A. Gebre, Z. Ryter, S. R. Humphreys, S. M. Ginsberg, S. P. Farrell, A. Kaufman, W. Capon, W. Robbins and K. Pochiraju, "A Multi-ball Dirve for Omnidirection Mobility," in *Technologies for Practical Robot Applications (TePRA), 2014 IEEE International Conference on*, Woburn, MA, 2014.

[5] H. Ghariblu, A. Moharrami and B. Ghalamchi, "Design and prototyping of autonomous ball wheel mobile robots," *Mobile Robots-Current Trends*, pp. 363-374, 2011.

[6] G. Seyfarth, A. Bhatia, O. Sassnick, M. Shomin, M. Kumagai and R. Hollis, "Initial Results for a Ballbot Driven with a Spherical Induction Motor," in *Robotics and Automation (ICRA), 2016 IEEE International Conference on. IEEE,*, Stockholm, Sweden, 2016.

[7] A. Özgür, W. Johal and P. Dillenbourg, "Permanent Magnet-Assisted Omnidirectional Ball Drive," in *Intelligent Robots and Systems (IROS), 2016 IEEE/RSJ International Conference on*, Daejeon Korea, 2016.

[8] C. Guy and W. Chung, "Springer Handbook of Robotics," in *Wheeled Robots*, Berlin Heidelberg, Springer, 2008, pp. 391-410.

[9] C. Mapelli and S. Barella, "Failure analysis of a ball transfer unit," *Engineering Failure Analysis*, vol. 14, no. 4, pp. 579-587, 20007.

[10] A. Bhatia, M. Kumagai and R. Hollis, "Six-Stator Spherical Induction Motor for Balancing Mobile Robots," in *Robotics and Automation (ICRA), 2015 IEEE International Conference on*, Seattle, WA USA, 2015.

[11] A. Özgür, W. Johal, F. Mondada and P. Dillenbourg, "Haptic-Enabled Handheld Mobile Robots: Design and Analysis," in *Proceedings of the 2017 CHI Conference on Human Factors in Computing Systems*, Denver, CO, 2017.

[12] "Selecting good features – Part III: random forests," [Online]. Available: http://blog.datadive.net/selecting-good-features-part-iii-random-forests/. [Accessed 15 February 2018].

[13] C.-C. Chung and C.-J. Lin, "LIBSVM: A Library for Support Vector Machines," *ACM transactions on intelligent systems and technology (TIST)*, vol. 2, no. 3, p. 27, 2011.

[14] "EMS software," [Online]. Available: https://www.emworks.com/product/EMS.

[15] B. A. Gebre and K. Pochiraju, "Ball Drive Configurations and Kinematics for Holonomic Ground Mobility," in *ASME International Mechanical Engineering Congress and Exposition*, Tampa, FL, 2017.